Imaging direct- as well as scattered-events in microseismic data using inverse scattering theory

Jyoti Behura & Roel Snieder
Center for Wave Phenomena, Colorado School of Mines, Golden, Colorado

ABSTRACT
Similar to surface reflection data, microseismic data also contain multiply-scattered events. They are especially prevalent in borehole microseismic data because of low attenuation. These scattered events, if not imaged accurately, can lead to the spurious microseismic hypocenters. Here, we introduce an imaging algorithm that accurately images not only the primary arrivals but also the multiply scattered events. The algorithm uses the exact Green's function computed using an iterative scheme based on inverse-scattering theory. Extraction of the Green's function, however, requires surface reflection data and a background velocity model. Imaging of surface microseismic data involves computation of the Green's function between the image point and the surface receivers and the application of an imaging condition to the data. Borehole-microseismic-data imaging, however, requires two additional steps – first, computation of the Green's function between the borehole receivers and the surface and second, computation of the Green's function between the image point and the borehole receivers using seismic interferometry. Tests on synthetic data show that our imaging algorithm not only locates the microseismic hypocenters accurately but also substantially reduces the number of spurious events.

1 MULTIPLE ISSUES

As seismic waves propagate through the subsurface, they undergo scattering because of the presence of heterogeneities (in velocity and density). In reflection seismology, events undergoing more than one episode of scattering are commonly referred to as *multiples*. Since multiples can result in spurious reflectors on images, the common practice is to predict and suppress them prior to imaging. However, since multiples also contain information about the subsurface heterogeneities, there is an increased effort towards using them in imaging instead of just discarding them.

Data recorded by passive sensors and during active microseismic monitoring also contain singly- and multiply-scattered events in addition to the direct arrival. Such data are commonly used to locate the sources of these hydraulic-fracturing induced microseismic events and thus compute an estimate of the *stimulated reservoir volume* and the evolution and geometry of induced fractures. Kirchhoff migration (Gajewski *et al.*, 2007) and reverse-time imaging (McMechan, 1982; McMechan *et al.*, 1983) are the imaging algorithms commonly employed to locate the microseismic sources. Under Kirchhoff migration, the image at any location is computed by first computing the direct-arrival traveltime from the image point to the receivers and then stacking the recorded data along this traveltime-curve. In reverse-time imaging, the recorded data is reversed in time and then injected into a smooth estimate of the subsurface velocity. If the velocity model is accurate, the direct arrivals will focus at the correct microseismic hypocenters.

In the above imaging algorithms, the scattered arrivals, however, will also focus at times and locations that do not correspond to the true initiation time of the microseismicity and the true hypocenters, respectively. They will result in numerous *false positives* particularly for large reflection coefficients. Many of the unconventional reservoirs with underlying/overlying sand-shale sequences can aggravate this issue. Scattering can be problematic for borehole monitoring, in particular, because of the large magnitudes of the multiples. Unfortunately, such false positives will not only lead to an overestimation of the stimulated reservoir volume but also result in a poor correlation of microseismicity with production. An example of this is clearly evident in the work of Roundtree & Miskimins (2011) where a sandstone is hydraulically fractured in a controlled exper-

iment. The microseismic data, when imaged, resulted in numerous hypocenters *outside* the sandstone block (Jennifer Miskimins, personal communication).

1.1 Exact Green's function necessary

One possibility to addressing the above scattering issue in microseismic data is to predict and suppress the scattered events on data prior to imaging. Unfortunately, this requires the complete knowledge of the velocity and density model; no data-driven approaches exist for predicting multiples in microseismic data. A comparison of reverse-time imaging with smoothed versus true velocity model is shown in Behura *et al.* (2013). The alternative approach is to use all the data and image the scattered arrivals (along with the direct arrivals) such that they focus at the correct hypocenters. This approach necessitates either the detailed and accurate knowledge of the velocity (and density) model or the knowledge of the Green's function. It is extremely challenging to obtain detailed information of the subsurface velocity and density. Well-logs can provide such detailed models but only locally. Seismic-inversion-derived subsurface models most commonly depict only the low-wavenumber background.

1.2 Inverse-scattering theory to the rescue

Wapenaar *et al.* (2011) propose a methodology for reconstructing the 3D Green's function between any "virtual source" in the subsurface and any location on the surface using only surface reflection data and a background velocity model. Their proposal is the 3D extension of the 1D iterative algorithm of Rose (2002b,a) who shows that in layered media, it is possible to focus all the energy at a particular time (or depth if the velocity is known) by using a complicated source signature. Rose's algorithm was also implemented on 1D seismic data by Broggini & Snieder (2012) who again show that a 'virtual source' response can be generated from surface reflection data alone. The background velocity model is used to compute the direct arrivals between the "virtual source" and the surface which are subsequently fed into an iterative algorithm to compute the Green's function. Details of the 1D algorithm are given in Rose (2002b,a); Broggini & Snieder (2012); the 3D algorithm can be found in Wapenaar *et al.* (2011) with the derivation given in Wapenaar *et al.* (2013).

Here, we propose to use the above iterative algorithm to reconstruct Green's function between the subsurface image points and the surface and use them in imaging the direct as well as the scattered events in microseismic data. We also introduce a methodology to image borehole microseismic data by combining the computed Green's functions with seismic interferometry.

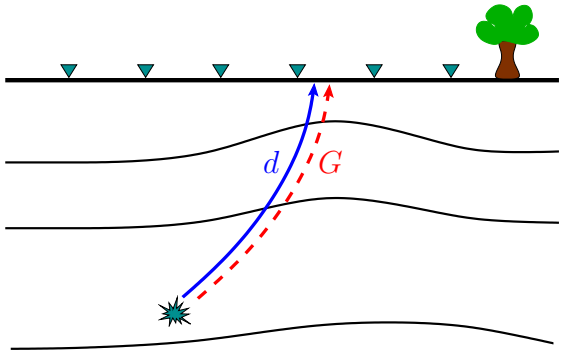

Figure 1. Schematic of the imaging algorithm applied to surface microseismic data. d represents the microseismic data recorded at the surface receivers (triangles) and G is the Green's function between any image point (denoted by the star) and the surface receivers obtained from the iterative algorithm.

2 SURFACE DATA IMAGING

The data recorded at a receiver $\mathbf{x_r}$ due to a source at some location $\mathbf{x}$ is given by

$$d(\omega; \mathbf{x_r}, \mathbf{x}) = S_{\mathbf{x}}(\omega)\, G(\omega; \mathbf{x_r}, \mathbf{x}), \tag{1}$$

where ω is the frequency, d is the data, $S_{\mathbf{x}}$ is the source signature at $\mathbf{x}$, and G is the Green's function. Note that $S_{\mathbf{x}}$ is not necessarily compact in time but can be complicated and of long duration. The source signature can therefore be computed by the application of an imaging condition to the data. A detailed description of the various imaging conditions used in microseismic imaging is given in Behura *et al.* (2013). Here, we use the 2D space-time cross-correlation imaging condition (Behura *et al.*, 2013):

$$S_{\mathbf{x}}(\omega) = \sum_{k_r} d(\omega, k_r)\, G^*(\omega, k_r), \tag{2}$$

where k_r is the wavenumber over the receiver coordinates and * represents complex-conjugation. Note that $S_{\mathbf{x}}$ obtained from equation 2 is a function of time which is different from the zero-time imaging condition commonly used in reverse-time imaging of microseismic data.

2.1 Sigsbee test

We test our imaging algorithm on the Sigsbee model (Figures 2) as it generates strong internal multiples. All the boundaries in the velocity model are absorbing.

The microseismic survey comprises of 367 receivers spread on the surface at an equal spacing of 75 ft. Two microseismic sources (Figure 2a) are used for generating the data; the initiation times of the left- and the right-source are 0.096 s and 3.36 s, respectively. Also, the left source has a higher amplitude than the right source.

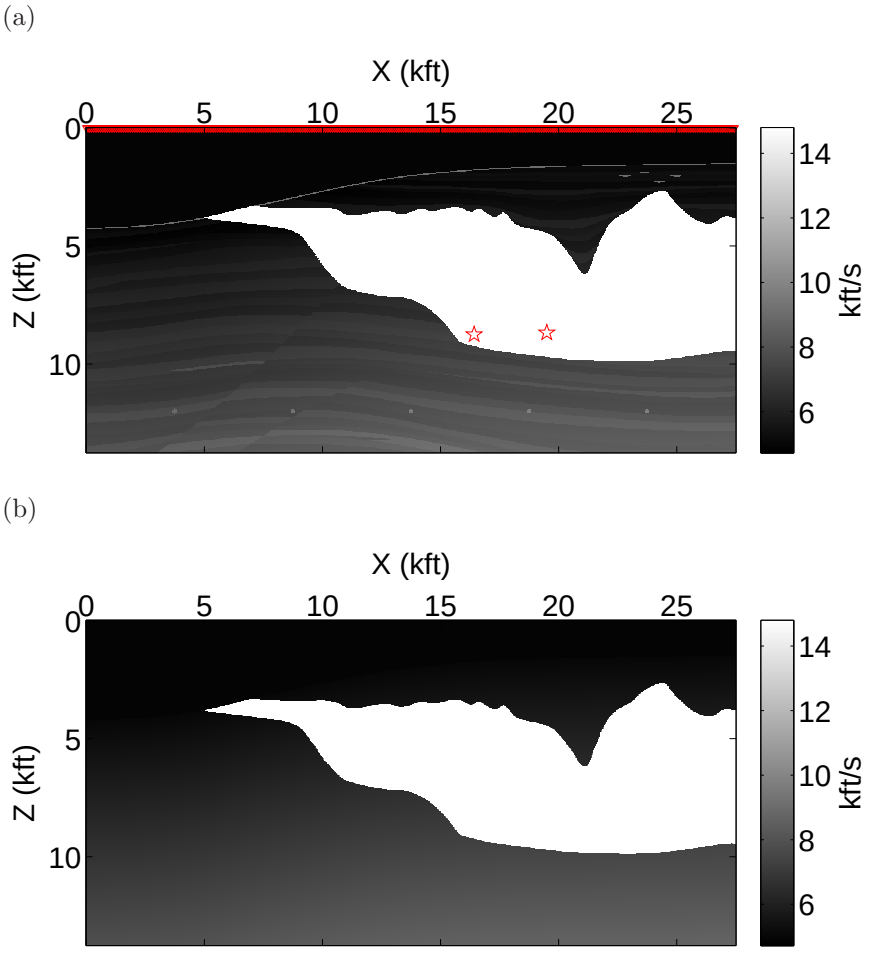

Figure 2. (a) The Sigsbee velocity model used in generating the microseismic data and the reflection seismic data. The two pentagons represent the microseismic hypocenters and the triangles represent the receivers. There are a total of 367 receivers spread on the surface at an equal spacing of 75 ft. (b) The smooth model used in imaging.

A fixed-spread receiver geometry is used for acquiring the surface reflection data; this spread coincides with the receiver geometry of the microseismic survey. Shot locations for the surface reflection data also coincide with the fixed-receiver spread. Thus, the surface reflection data comprises of 357 shot gathers, with each shot gather containing 367 traces.

Figure 3a shows the image of the two microseismic sources obtained using the imaging methodology introduced here. Behura *et al.* (2013) argue that the image of microseismic data should be displayed as a function of space as well as time because the sources can be extended in both space and time. The images in Figure 3 correspond to specific depth slices of the $z-x-t$ image cube. Note that both microseismic sources have been imaged at the correct time and also the right location; even the relative amplitudes of the two sources are preserved. More importantly, there are no spurious events in the image. The reverse-time image (Figure 3b), on the other hand, contains numerous events most of which are spurious. The left source is faintly visible, albeit its amplitude is much smaller than the spurious events; the right source is barely discernible. Some of these spurious events can be eliminated by smoothing the salt body; this will, however, lead to mis-positioning of the microseismic hypocenters (in time and space). Therefore, in the presence of multiples, reverse-time imaging can yield numerous false positives in identification of microseismic sources. For such data containing multiples, the inverse-scattering imaging method introduced here should be the algorithm of choice.

3 BOREHOLE DATA IMAGING

Like surface microseismic data, borehole data can also be imaged using the Green's function G_{ib} between the

(a)

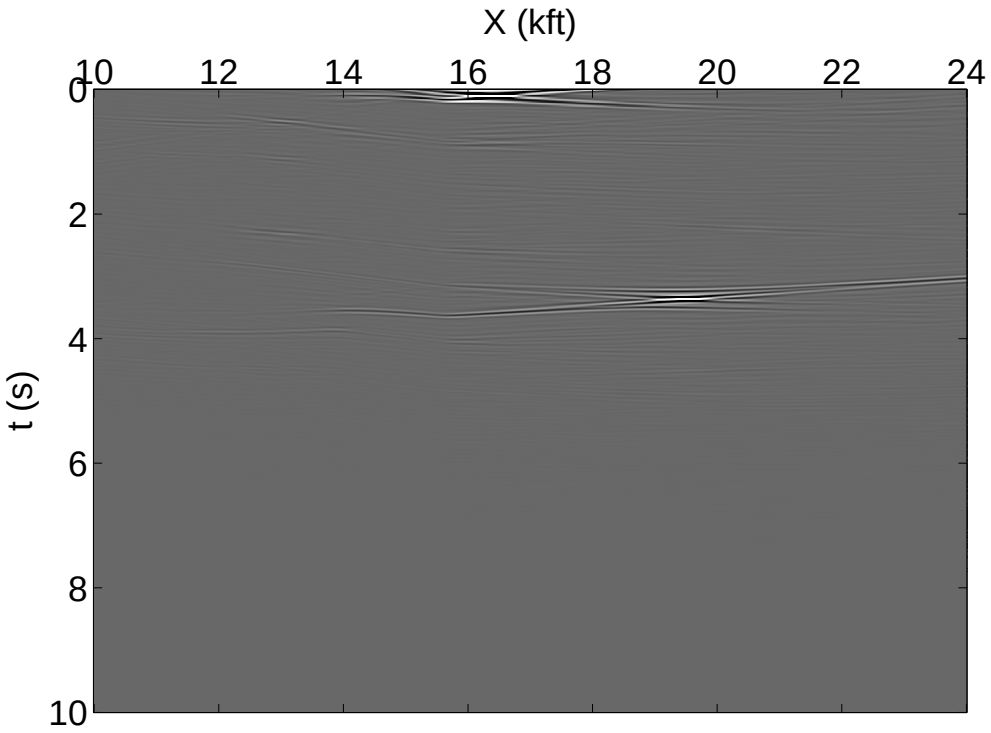

(b)

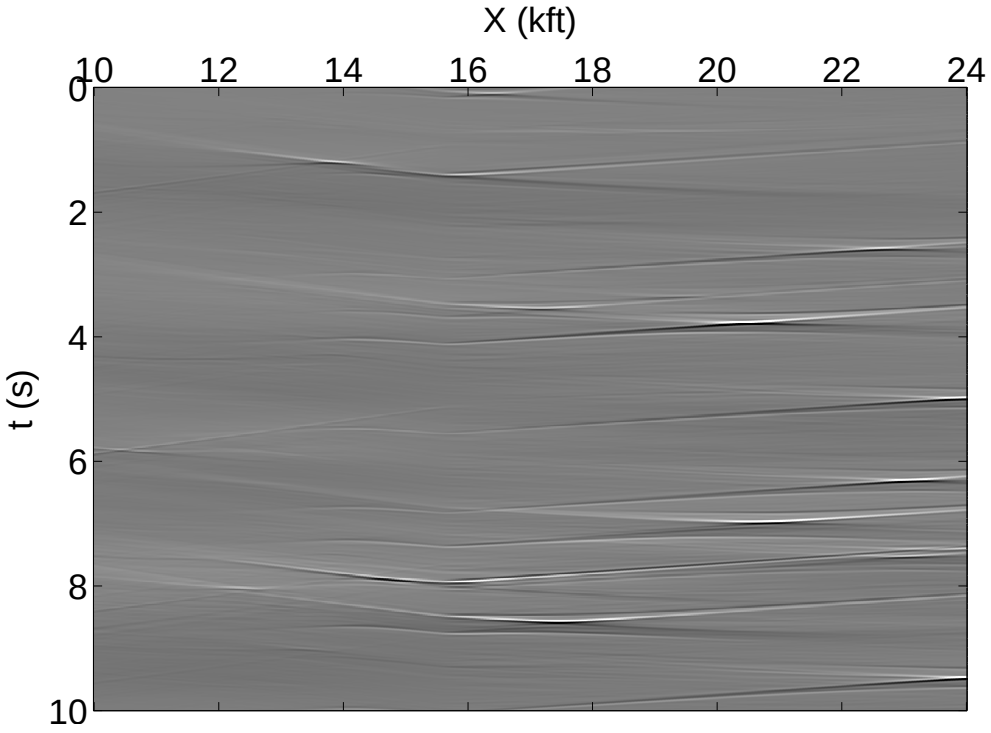

Figure 3. Images of the microseismic sources shown in Figure 2a obtained using the inverse-scattering-theory (a) and reverse-time imaging (b). The images correspond to a depth of 5700 ft. Two iterations were used in computing G using the iterative algorithm.

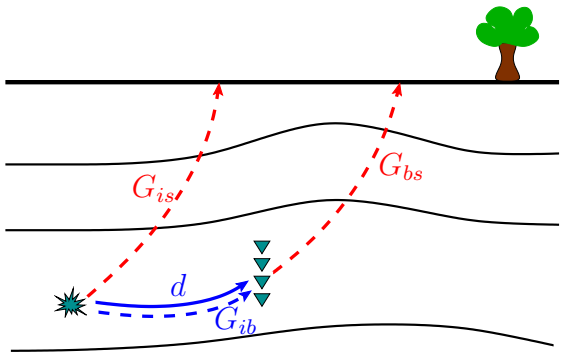

Figure 4. Schematic of the borehole microseismic data imaging algorithm based on Green's function retrieval using the iterative scheme. The triangles represent borehole receivers and the star is the microseismic hypocenter. d is the borehole microseismic data, G_{is} represents the Green's function between the image point and the surface, G_{bs} represents the Green's function between the borehole receivers and the surface, and G_{ib} is the Green's function between the image point and the borehole receivers. G_{is} and G_{bs} are computed from the surface reflection data using the iterative scheme, while G_{ib} is retrieved from G_{is} and G_{bs} using seismic interferometry.

image point and the borehole receivers. G_{ib}, however, cannot be directly computed using the iterative algorithm of Rose (2002b,a) because the borehole receivers are in the interior of the medium and because of the absence of reflection data with both shots and receivers in the borehole.. To compute G_{ib}, we use the following algorithm:

(i) compute G_{bs}, the Green's function between the borehole receivers and the surface receivers using the iterative algorithm

(ii) similarly, compute G_{is}, the Green's function between the image point and the surface receivers using the iterative algorithm

(iii) obtain G_{ib} from G_{is} and G_{bs} using seismic interferometry (Wapenaar & Fokkema, 2006) based either on cross-correlation, deconvolution, or multi-dimensional deconvolution (Wapenaar *et al.*, 2008).

Thereafter, we obtain the microseismic image by application of the following imaging condition to the data:

$$S_{\mathbf{x}}(\omega) = \sum_{k_r} d_{bh}(\omega, k_r)\, G^*_{ib}(\omega, k_r), \tag{3}$$

where d_{bh} is the borehole microseismic data and $S_{\mathbf{x}}$ is the source signature at $\mathbf{x}$.

3.1 Layer-cake test

We test the above borehole-microseismic-data imaging algorithm on a layer-cake velocity model (Figure 5a). The velocity model is constructed by extrapolating laterally a well-log velocity profile from Pennsylvania (Trenton Black River Project – Appalachian Basin).

Similar to the Sigsbee example above, all the boundaries are absorbing. The microseismic data is generated for a single source location shown in Figure 5a and recorded at the 22 borehole receivers (Figure 5a). The initiation time of the source is 0.2 s. The surface reflection data is acquired on a fixed-receiver spread with 461 receivers equally spaced at 25 m intervals. The shot points coincide with the receiver spread.

In order to perform imaging using our methodology, we compute G_{is}, G_{bs}, and G_{ib} as described above. Two iterations were used in computing G_{is} and G_{bs} using the iterative scheme. Thereafter, we apply imaging condition 3 on the borehole microseismic data. The recovered image for the true source depth level is shown in Figure 6a. Note that the focusing is better than that for reverse-time imaging (Figure 6b). In addition, the spurious events have been largely eliminated.

4 ROLE OF BACKGROUND VELOCITY

The background velocity model is used to compute the direct arrivals which are thereafter input into the iterative algorithm to calculate the Green's function Wapenaar *et al.* (2011). As suggested in (Wapenaar *et al.*, 2011), microseismic events visible on the data can also be substituted for direct arrivals. However, since we neither know the hypocenters of such events and nor are there microseismic sources everywhere, it is impractical to use visible events for direct arrivals.

A viable solution would be to use arrivals from perforation shots as direct arrivals because we already know the perforation locations. If the medium is laterally homogeneous (commonly true for unconventional reservoirs), one could use a well-log-derived velocity profile to compute direct arrivals for other image points from the perforation-shot events using upward/downward wavefield continuation. Such an approach would alleviate the need for a background velocity model.

As mentioned above, Green's function retrieval using the iterative algorithm of Rose (2002b,a); Wapenaar *et al.* (2011); Broggini & Snieder (2012) uses surface reflection data. Since the density information is already contained in the reflection data, the events corresponding to the scattered waves in the reconstructed Green's functions will have accurate amplitudes. This greater accuracy should further help in reducing false positives in microseismic imaging and also yield more accurate source signatures.

(a)

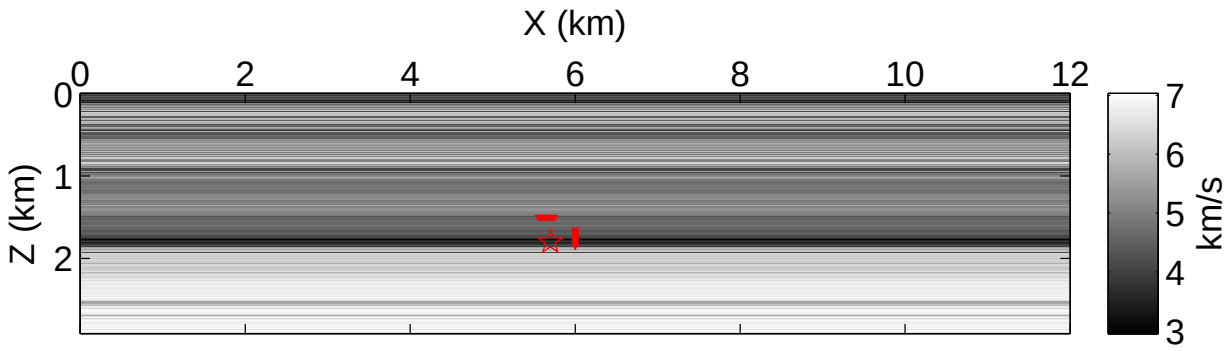

(b)

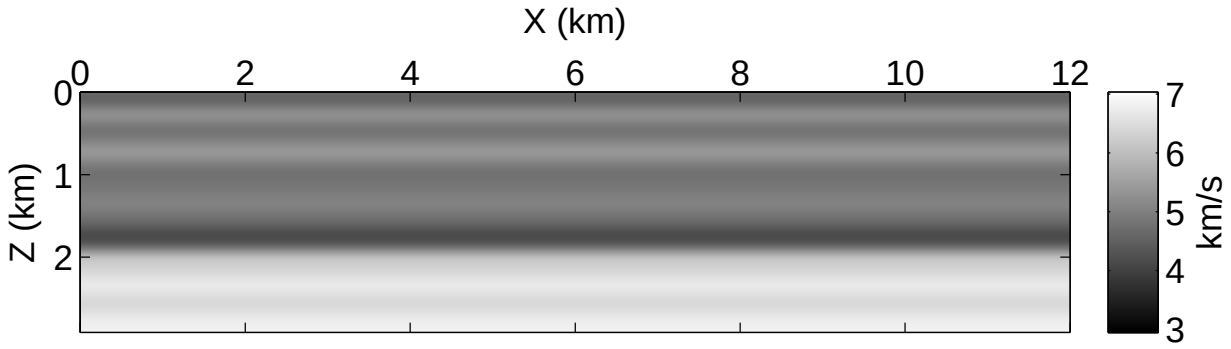

Figure 5. (a) The layer-cake velocity model used in generating borehole microseismic data and the surface reflection data. The pentagon represents the hypocenter of the microseismic source and the triangles represent the borehole receivers. The borehole receivers are emplaced as two separate arrays – one horizontal and the other vertical. Each array comprises of 11 receivers that are evenly spaced at 20 m intervals. (b) The smooth velocity model used in imaging.

5 DISCUSSION

Microseismic imaging using conventional imaging algorithms uses only the recorded data and a background velocity model. The imaging technique described here, however, needs surface reflection data in addition. Nonetheless, it is becoming common practice to acquire both surface reflection data and microseismic data for detailed characterization of unconventional plays. Moreover, the iterative algorithm requires an accurate knowledge of the source signature in the surface reflection data. The source function is known in many cases (e.g. vibroseis acquisition) or can be recorded in others (e.g. air-gun source). Where, the source signature is unknown, deterministic methods such as Virtual Real Source (Behura, 2007) should be used to compute it.

The iterative algorithm of Rose (2002b,a); Wapenaar *et al.* (2011); Broggini & Snieder (2012) can successfully recover the Green's function when all the scattering is in the interior of the medium. In the presence of a free-surface, however, the algorithm fails to compute the exact Green's function. Using a modified algorithm, Singh *et al.* (2013) show that the exact Green's function can be extracted even in the presence of free-surface reflections. This modified algorithm might be used for imaging microseismic data containing free-surface multiples.

The imaging algorithm introduced here is substantially more computationally intensive than conventional algorithms such as reverse-time imaging and Kirchhoff imaging. Computation of the direct arrivals is the primary driver of the cost. There are two strategies for computing the direct arrivals between the image points and the surface receivers. First – the direct arrivals for each image point can be computed on the fly while the code is being executed. The number of forward computations will equal the number of image points. This will require significant processor power but have minimal disk input-output costs. Second – since there are far fewer receivers than image points, one could compute the direct arrivals for all image points from each receiver location independently and then store them to the disk. Thus the number of forward computations will equal

(a)

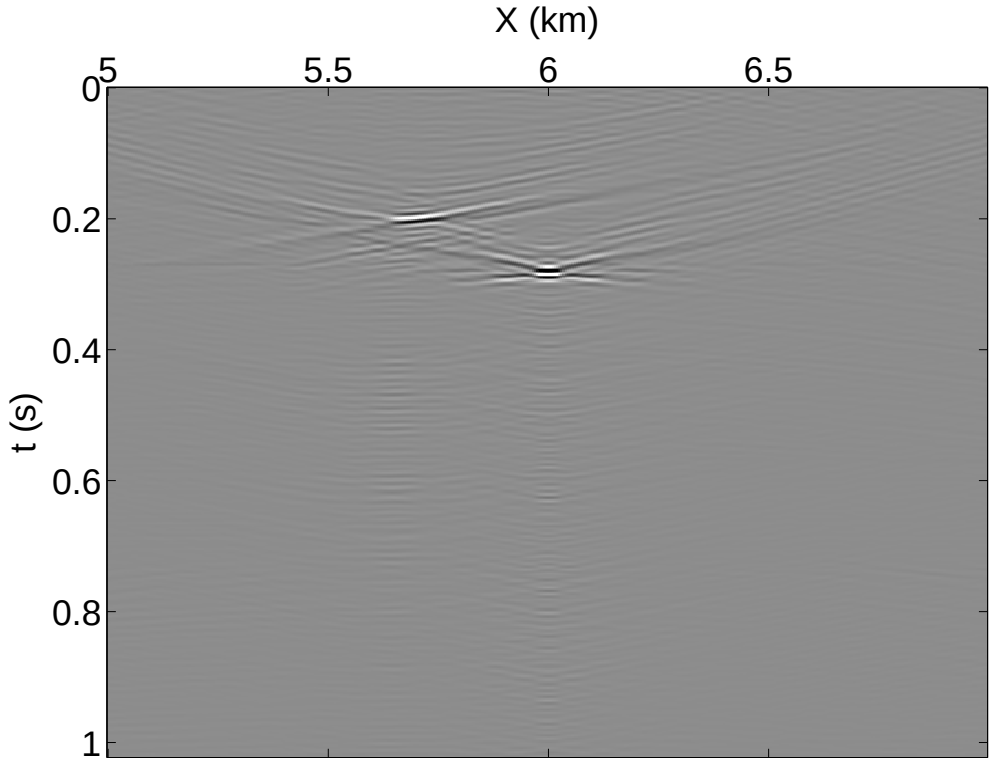

(b)

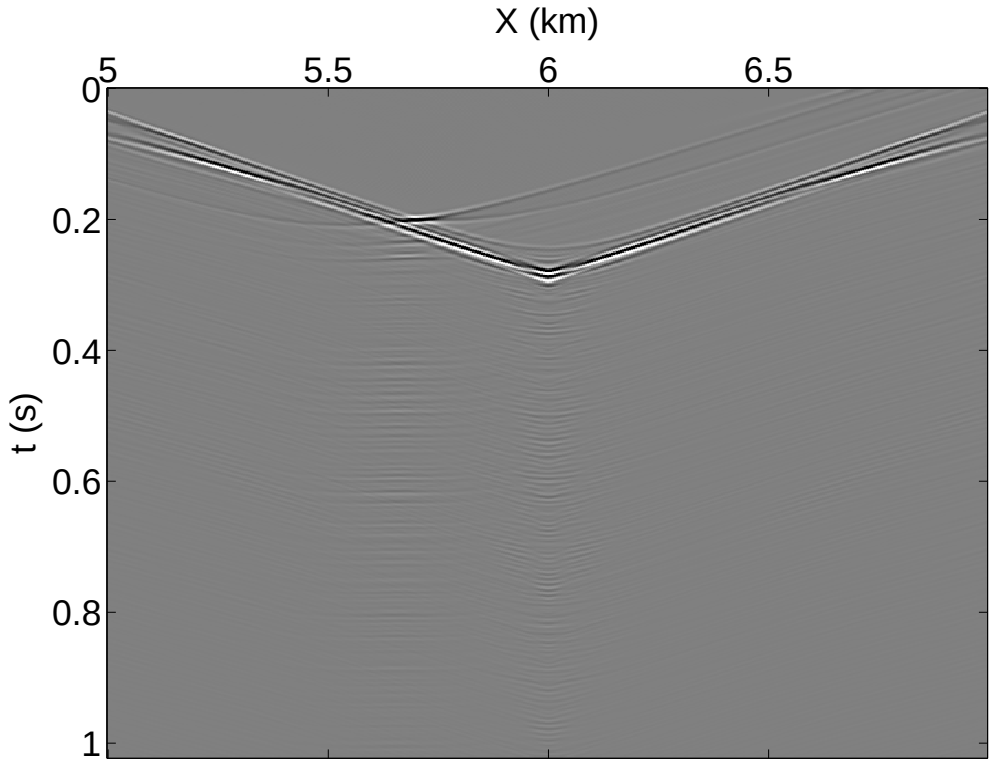

Figure 6. Images of the microseismic source shown in Figure 5a obtained using the inverse-scattering-theory based algorithm (a) and reverse-time imaging (b). The images correspond to the true depth of the microseismic hypocenter (1800 m). The event at t =0.3 s and x =6 km in (a) corresponds to the location of the vertical receiver array. The same event manifests as a linear moveout in (b).

the number of receivers. Because of reciprocity, one can then read the direct arrivals from the disk for each image point; this, however, involves substantial disk input-output operations. Based on the number of receivers versus the number of image points, one can choose either of the above two strategies.

The iterative algorithm of Rose (2002b,a); Wapenaar *et al.* (2011); Broggini & Snieder (2012) is applicable to only acoustic wave propagation. In the presence of strong shear waves in microseismic data (especially in borehole recordings), all imaging algorithms will fail to properly characterize the microseismicity. Therefore, shear waves should be suppressed in the data before imaging. Shear-wave suppression is more critical for borehole data and less so for surface acquisition because of the strong near-surface attenuation.

6 CONCLUSIONS

Imaging of microseismic data in the presence of multiples will result in numerous false positives i.e. identification of spurious microseismic hypocenters. In order to image such data accurately, we have developed an algorithm that uses exact Green's function derived using an iterative scheme based on inverse-scattering theory. Both surface- and borehole-microseismic data can be imaged using our approach. Tests on synthetic data show that our approach can reduce false positives significantly as well as improve the focusing of the microseismic hypocenters.

ACKNOWLEDGMENTS

We thank Farnoush Forghani and Satyan Singh for many discussions. Support for this work was provided by the Consortium Project on Seismic Inverse Methods for Complex Structures at Center for Wave Phenomena.

References

Behura, J. 2007. Virtual Real Source. *SEG Technical Program Expanded Abstracts*, 2693–2697.

Behura, J., Forghani, F., & Bazargani, F. 2013. Improving microseismic imaging: role of acquisition, velocity model, and imaging condition. *CWP Project Review*, **754**, 77–86.

Broggini, F., & Snieder, R. 2012. Connection of scattering principles: a visual and mathematical tour. *European Journal of Physics*, **33**(3), 593.

Gajewski, D., Anikiev, D., Kashtan, B., Tessmer, E., & Vanelle, C. 2007. Localization of seismic events by diffraction stacking. *SEG Technical Program Expanded Abstracts*, 1287–1291.

McMechan, G. A. 1982. Determination of source parameters by wavefield extrapolation. *Geophysical Journal of the Royal Astronomical Society*, **71**, 613–628.

McMechan, G. A., Luetgert, J. H., & Mooney, W. D. 1983. Imaging of earthquake sources in Long Valley Caldera, California. *Bulletin of the Seismological Society of America*, **75**, 1005–1020.

Rose, J. H. 2002a. *Time reversal, focusing and exact inverse scattering*. 1 edn. Springer-Verlag, Berlin. Pages 97–105.

Rose, J. H. 2002b. Single-sided autofocusing of sound in layered materials. *Inverse Problems*, **18**, 19231934.

Roundtree, R., & Miskimins, J. 2011. Experimental Validation of Microseismic Emissions from a Controlled Hydraulic Fracture in a Synthetic Layered Medium, SPE 140653. *In: SPE Journal*.

Singh, S., Snieder, R., & Behura, J. 2013. *Reconstruction of the exact Green's function in the presence of a free surface*.

Wapenaar, K., & Fokkema, J. 2006. Green's function representations for seismic interferometry. *Geophysics*, **71**(4), SI33–SI46.

Wapenaar, K., van der Neut, J., & Ruigrok, E. 2008. Passive seismic interferometry by multidimensional deconvolution. *Geophysics*, **73**(6), A51–A56.

Wapenaar, K., Broggini, F., & Snieder, R. 2011. A proposal for model–independent 3D wave field reconstruction from reflection data. *SEG Technical Program Expanded Abstracts*, **30**(1), 3788–3792.

Wapenaar, K., Broggini, F., Slob, E., & Snieder, R. 2013. Three-Dimensional Single-Sided Marchenko Inverse Scattering, Data-Driven Focusing, Green's Function Retrieval, and their Mutual Relations. *Phys. Rev. Lett.*, **110**(Feb), 084301.